SAND2013-5393C

POSITIVE-POLARITY ROD-PINCH EXPERIMENTS ON THE RITS-6 ACCELERATOR

J. J. Leckbee†, S. R. Cordova, M. D. Johnston, B. V. Oliver, T. J. Webb, and D. R. Ziska
Sandia National Laboratories, Albuquerque, NM*

V. L. Bailey, P. A. Corcoran, I. D. Smith, and B. A. Whitney,
L-3 Communications Pulse Sciences, San Leandro, CA

Abstract

RITS-6 is an inductive voltage adder based accelerator used for radiographic diode research and development. A recent experiment was conducted to demonstrate that a negative polarity induction voltage adder could operate in positive polarity, at reduced voltage, with minimal reconfiguration and maintenance. Circuit simulations, 2-D electrostatic field calculations, and particle-in-cell simulations were used to evaluate operation of RITS-6 in positive polarity and design hardware modifications. Changes to the RITS-6 accelerator during the conversion from negative-polarity high voltage (5-11 MV) output to positive-polarity low voltage (2-3 MV) output are discussed. The first positive polarity rod-pinch experiment generated 3.5 rad from a 1-mm spot size, comparable to previously published rod-pinch experiments on positive polarity accelerators.

I. INTRODUCTION

The RITS-6 accelerator is typically configured to drive electron beam diodes with voltages ranging 5-11 MV [1], [2]. Two different MITL impedance options exist so that experiments with a 40-Ω MITL are conducted with a load voltage of 5-7 MV and with a 80-Ω MITL and load voltage of 7-11 MV. All experiments were previously conducted in negative polarity. Conversion of an IVA to positive polarity typically requires significant maintenance [3].

The design process for this experiment included an analysis of every major component of the accelerator. The goals of the analysis were to evaluate any increase in electrical stress that could lead to component failure and evaluation of operating points to determine if the experiment would be possible. The first half of this paper discusses the analysis of the accelerator and design of new hardware that was required to convert the accelerator to positive polarity. The second half of the paper summarizes the subsequent positive-polarity rod-pinch experiment, the first positive polarity experiment on the RITS accelerator.

II. CONVERSION TO POSITIVE POLARITY

Conversion of the RITS-6 accelerator to positive polarity without reversing the orientation of the voltage adder cells allows for quick setup and conversion of the accelerator but adds additional stresses to the accelerator that required evaluation. Each major component of the accelerator had to be evaluated to determine if stresses would increase the probability of component failure and also to verify that the new operating points would be within the operating range of each component. Circuit simulations of the full accelerator were used to predict voltage levels on various components. Two-dimensional electrostatic simulations were used to evaluate field stresses on each component. The conversion from negative to positive polarity required less than two weeks of maintenance and only required manufacturing of a few new components discussed below.

A. Marx Generator

Previous testing of the Marx generator had been conducted with SF_6 filled spark gap switches and capacitor charge voltage ranging from 50-90 kV. Circuit simulations of the accelerator indicated that the Marx would need to be fired at 25-30-kV charge to deliver 2-3 MV to the diode load. Extrapolatinon from previous operating points indicated that the Marx could not be successfully fired at this low voltage with SF_6 filled spark gaps. The Marx was converted to use pressurized dry air instead of SF_6. A self-break curve for the Marx switches with dry air was used to determine the required pressures and the Marx was tested into a resistive load for charge voltages of 25-50 kV to verify proper operation and acceptable jitter at each new operating point.

* Sandia National Laboratories is a multi-program laboratory managed and operated by Sandia Corporation, a wholly owned subsidiary of Lockheed Martin Corporation, for the U.S. Department of Energys National Nuclear Security Administration under contract DE-AC04-94AL85000.
† Joshua.Leckbee@sandia.gov

B. Intermediate Storage Capacitors

The RITS-6 Marx is discharged into two water filled intermediate storage capacitors to begin the pulse compression. The capacitors are a coaxial geometry and in negative polarity, the center conductor which has the highest field stress, is the cathode. Water breakdown experiments have shown approximately a factor of two increase in voltage hold-off in water when the enhanced electrode is the cathode compared to the anode [4]. Reversing the Marx polarity reverses the polarity of the large water capacitors so that the highest field stress is on the anode. Two dimensional electrostatic simulations were used to determine the field stress on the center conductor of the water capacitors. A method to calculate the failure probability of water insulated components was developed by Elizondo in which he used an integral approach to calculating the probability of failure [5]. This method is somewhat more conservative than estimating the stressed area of the electrodes and calculating the probability of failure. Using the integral approach and assuming a Marx charge of 25 kV, we calculated a probability of failure of one of the two capacitors at 2.3×10^{-7} for a shot with normal switch timing and 3.0×10^{-5} if the output switch did not fire. This stress level was deemed sufficiently low for this experiment. No failures were observed during the 30 shots fired in positive polarity.

C. Laser Triggered Gas Switches

Each of the two intermediate storage capacitors is connected to a laser triggered gas switch at its output. The gas switches are designed to run at voltages up to 3 MV. The RITS-6 circuit simulation predicts that the gas switch needs to fire when the voltage on the intermediate storage capacitor is 1 MV. Data was available from several operating pressures ranging from 20 psig for a capacitor charge of 1.75 MV to 46 psig at 2.9 MV. Extrapolating down to a charge of 1 MV requires that the switches be pressurized to 2-5 psig. The switches were successfully run at 4 psig and triggered with a jitter of about 3 ns, only slightly higher than the normal 1.5-2 ns jitter when running at higher voltage. There was however an increase in the runtime of the switches which required that the timing of the lasers be adjusted to maintain proper timing of the accelerator.

D. Pulse Forming Lines

Each of the intermediate storage capacitors discharges through a laser triggered gas switch and charges three coaxial water filled pulse forming lines (PFL). The first section of the PFL is charged to approximately the same voltage as the intermediate storage capacitors, but in about 200 ns compared to the $> 1\mu s$ charge time of the intermediate storage capacitors. The same integral method of estimating the probability of failure discussed above was used to analyze the PFL for the case where the Marx charge is 25 kV. The estimated probability that one of the six PFLs would fail was 2.5×10^{-6} for normal switch timing and 5.0×10^{-5} if the PFL water switch did not fire. As with the intermediate storage capacitor, there were no failures observed during the 30 shots fired in positive polarity.

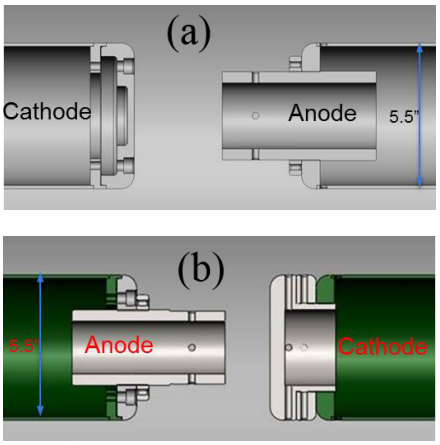

Figure 1. Drawings of the negative and positive polarity electrodes in the PFL water switch. (a). Negative polarity electrodes. (b). Positive polarity electrodes with the new hardware shown in gray and the existing PFL center conductors in green.

E. PFL Water Switches

Each PFL contains an untriggered, or self-breaking, water switch; a water peaking switch; and an oil filled prepulse suppression switch. The electrodes on each of these switches can be adjusted to change the gap length and thus the voltage at which the switch will close. The main self-breaking switch sets the timing of the PFL and thus the jitter of this switch is the most important of the three switches. Experiments with various switch electrode geometries on the RITS-3 PFL switches showed that the switch jitter was lowest with a flat plane cathode and a field enhanced anode [6]. The existing PFL electrodes, shown in Fig. 1 a, can be removed from the PFL center conductors, but they cannot be swapped to invert the polarity. A new set of electrodes, shown in Fig 1 b, was designed to mate without modification to the existing PFL conductors. The design is very similar to the original hardware with a threaded anode to adjust the switch gap and a flat plate on the cathode. The required gap was determined by extrapolation from previous switch operating points. The PFL switch jitter was 2.2-5.0 ns compared to 2.9-5.7 ns for a recent set of shots in negative polarity at higher voltage with new switch electrodes. No adjustments were made to the water peaking switches or the oil prepulse suppression switches.

F. Voltage Adder Cells

The voltage adder cells are filled with transformer oil. For geometries with low field enhancement, the breakdown strength of oil in negative polarity is roughly 40%

higher than positive polarity [7]. The vacuum insulator stack in each cell is designed for operation in negative polarity and consists of a stack of 11 rexolite ring insulators with a 45° taper on the vacuum side of the insulator. The flashover voltage of shaped insulators has shown that the voltage hold-off of an insulator with a 45° taper where the thicker side of the insulator is at the anode is 50-75% of the voltage breakdown voltage when the thicker side of the insulator is at the cathode [8], [9]. The RITS-6 cells have been tested as high as 1.9 MV each without insulator flashover or failure in the oil section of the cell. The cell could thus be used in positive polarity up to about 0.9 MV per cell. In the positive polarity experiment discussed here, the cell voltage is less than 0.5 MV, well below the limit for positive polarity.

G. Vacuum Output Transmission Line

Previous experiments with rod-pinch diodes in positive polarity have been conducted on accelerators with little or no electron emission in the output transmission line [10], [11]. Electrostatic calculations of the RITS-6 vacuum output line were used to identify regions of field enhancement that could lead to significant electron emission. One such area that was identified is the downstream corner of the cell AK gap. Figure 2 shows a plot of the field stress where the dark blue regions are the metal conductors. The shaped surface in the upper left is the anode of the cell and the cathode is in the upper right portion of the plot. The tapered conductor at the bottom is the outer edge of the center conductor of the coaxial line. The field stress on the sharp cathode corner on the downstream side of the cell exceeds 500 kV/cm. A new field shaper was designed that could be installed in each cell without disassembling the cell and is shown in Fig. 2 b. The field shaper reduces the peak field stress to less than 240 kV/cm if the cell voltage reaches 500 kV and the center conductor voltage reaches 3.0 MV. In addition to the high field stress at the output of each cell, there is a field enhancement on the outer cathode conductor near the vacuum pumping ports located about half way between the last cell and the diode. This region could not be modified without significant accelerator maintenance. The new field shapers were expected to reduce but not fully prevent electron emission in the output line.

III. ROD-PINCH DIODE RESULTS

After conversion from negative to positive polarity, 20 rod-pinch shots were fired. Fifteen of the shots were fired with a Marx charge of 25 kV, which we had predicted from circuit simulations would generate about 2 MV at the load. At the end of the experiment, the last five shots were fired with a Marx charge of 30 kV, a 20% increase in charge voltage. The geometry and operation of the rod-pinch diode in positive polarity has been detailed in several papers and is not treated in detail here [11]–[14]. Shots

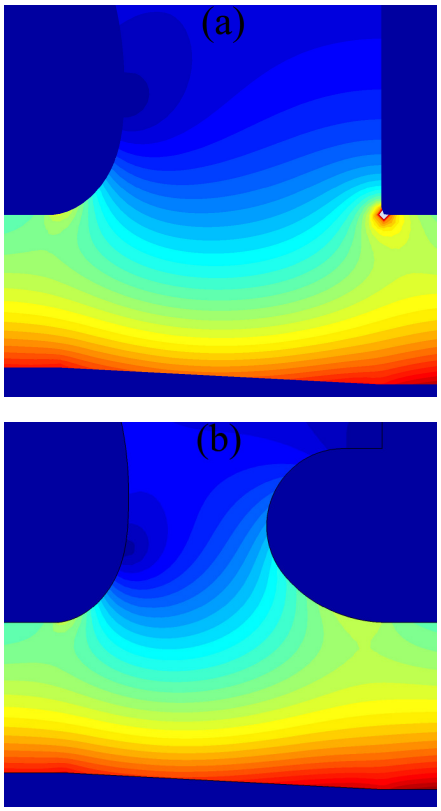

Figure 2. Electrostatic field plots of the electric field magnitude at the output of the last IVA cell. (a). Original design with sharp cathode edge. (b). New field shaper design.

reported here use a 0.75 mm diameter solid tungsten rod that tapers to 0.25 mm over the last 5 mm.

The plots in Fig. 3 show the anode and cathode currents measured in the output transmission line about half way between the last cell and the diode. During the rising edge of the pulse, the anode and cathode currents match. At the peak of the pulse the anode current is up to 7 kA higher than the cathode current. The difference between the anode and cathode currents represents electron current that has been emitted from the cathode and is magnetically insulated and flowing toward the load. Electron emission from the cathode affects the operation of capacitive voltage monitors and prevents a direct measurement of the voltage in the output line.

The x-ray dose rate is measured using PIN diodes fielded near the accelerator axis and about 1 m from the tip of the rod. The PIN diode is calibrated by integrating the output and comparing the integrated dose to the dose measured by thermoluminescent dosimeters (TLD) fielded at the same distance from the diode. The TLDs are fielded inside an aluminum block with approximately 2.54 cm of aluminum shielding in all directions. The calibrated PIN diode dose rate measurement is shown in Fig. 4.

Calculations of x-ray dose production from a rod-pinch diode by Rose et al. provide an equation relating the

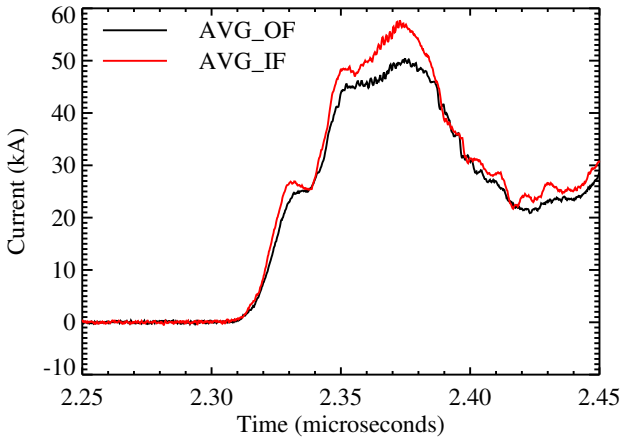

Figure 3. Plot of the MITL currents on the outer cathode and the inner anode. The difference between the two represents insulated electron flow current.

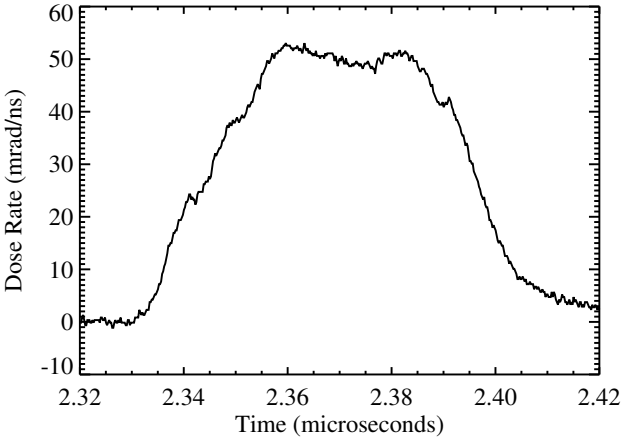

Figure 4. Plot of the x-ray dose rate measured by a PIN diode 1-m from the x-ray source near the accelerator axis.

diode voltage and current to the x-ray dose rate measured through 2.54 cm of aluminum shielding [15]

$$\frac{dD}{dt} \approx 0.61 I_D V_D^{1.25}. \quad (1)$$

Equations such as this one are commonly referred to as radiographers equations. Using the measured diode current and the calibrated x-ray dose rate, we can use this equation to calculate the diode voltage, shown in Fig. 5. Using this method the peak voltage is about 1.7-1.8 MV.

Another method that has been used on previous RITS-6 experiments to determine the diode voltage is to run a series of PIC simulations to match experimental data [16]. When the PIC simulation is setup so that the simulated anode and cathode currents match experimental currents at multiple locations in the output transmission line and multiple locations near the diode, then the PIC simulation predicted voltage should be representative of the diode voltage in the experiment. Two dimensional PIC simulations were run of the entire vacuum line including all six voltage adder cells and the diode. The electron emission

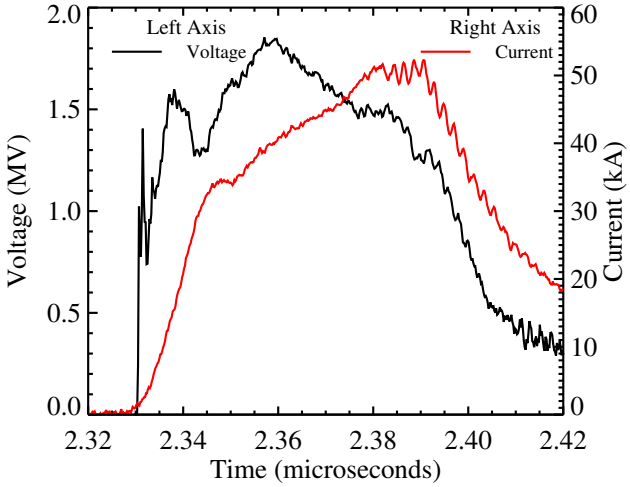

Figure 5. Plot of the measured cathode current at the diode and the diode voltage calculated from the current and dose rate.

threshold and diode impedance were varied to improve agreement with experimental data. The simulations suggest a peak diode voltage of 1.7 MV, in good agreement with the voltage calculated from the radiographers equation.

The total dose from the 25-kV Marx shots was typically about 2.5 rad when measured through 2.54 cm of aluminum shielding. The x-ray source spot size was measured using a rolled edge and image plate as described in ref. [16]. The source spot size is quoted here as the FWHM of the line spread function (LSF) multiplied by 1.4. The average LSF spot size on these shots is 0.9 mm.

For the last five shots fired in the experiment, the Marx charge voltage was increased from 25 kV to 30 kV in an attempt to increase the diode voltage to 2 MV and increase the x-ray dose production. In the lower voltage shots, the diode impedance decreases throughout the pulse. The decreasing diode impedance is seen in Fig. 5 as a decreasing diode voltage accompanied by increasing diode current. In the higher charge voltage shots, the cathode hole diameter was varied from 8.9 mm to 12 mm (the lower voltage shots all use a 8.9 mm diameter hole). Increasing the cathode hole diameter while maintaining a constant anode diameter increases the impedance of the diode [11]. Figure 6 shows the diode current and calculated diode voltage for a shot with 30 kV Marx charge and a 12 mm diameter cathode hole. In this shot, the calculated diode voltage peaks briefly at 2 MV and unlike the shots with smaller diameter cathode hole, the diode voltage does not decrease during the output pulse.

As shown in Fig. 7, the x-ray dose rate is higher than the measured dose rate on the lower voltage shots. The PIN signal also shows a sharp rise in dose rate near the end of the pulse. The total integrated x-ray dose is 3.4 rad measured through 2.54 cm of aluminum. The x-ray source spot size increased from 0.9 mm to 1.0 mm with the

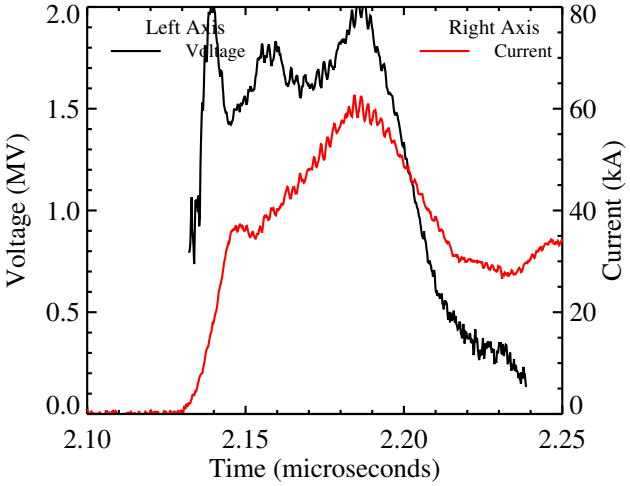

Figure 6. Plot of the diode cathode current and the calculated diode voltage for a shot with 20% higher Marx charge voltage.

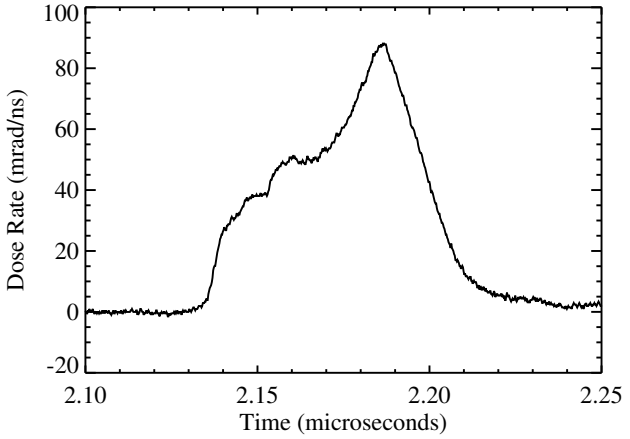

Figure 7. Plot of the x-ray dose rate for a show with 20% higher Marx charge voltage.

increase in voltage. The resulting dose and spot size are similar to those quoted for the Cygnus accelerator [14]. The lower x-ray dose production on RITS-6 is a result of the 10% lower diode voltage.

IV. CONCLUSION

The RITS-6 accelerator was successfully converted to run at significantly reduced voltage in positive polarity with minimal modification and maintenance. A full analysis of the accelerator was conducted to determine switch operating pressures and gaps and to verify that the electrical stress on the various components would not exceed design parameters. New hardware included electrodes to reverse the polarity of the PFL switches and field shapers to reduce field stress in the voltage adder cells.

The first positive-polarity rod-pinch diode experiment was conducted on RITS-6, consisting of a total of 20 shots. The current was measured in the output transmission line and in the diode. The diode voltage was calculated using the rod-pinch diode radiographers equation and confirmed using PIC simulations of the full vacuum section of the accelerator. The diode x-ray dose and spot size are consistent with the slightly decreased diode voltage compared to published results from the Cygnus rod-pinch diode.

V. REFERENCES

[1] D. Johnson, *et al.*, "Status of the 10 MV 120 kA RITS-6 inductive voltage adder," in *Proc. 15th IEEE Int. Pulsed Power Conf.*, Monterey, CA, 2005, pp. 314–317.

[2] J. Leckbee, *et al.*, "RITS-6 output pulse shape modifications," in *Proc. 16th IEEE Int. Pulsed Power Conf.*, Albuquerque, NM, 2007, pp. 1264–1267.

[3] R. J. Allen, *et al.*, "Conversion of Mercury (a 2-TW inductive voltage adder) to positive polarity," in *Proc. 17th IEEE Int. Pulsed Power Conf.*, Washington, DC, 2009, pp. 1171–1175.

[4] J. C. Martin, "Nanosecond pulse techniques," *Proc. IEEE*, vol. 80, no. 6, pp. 934–945, 1992.

[5] J. M. Elizondo, T. H. Martin, K. W. Struve, and L. F. Bennett, "The Z-20 reliability calculations," in *Proc. 14th IEEE Int. Pulsed Power Conf.*, Dallas, TX, 2003, pp. 895–898.

[6] E. Puetz, I. Molina, S. Portillo, S. Cordova, D. L. Johnson, and P. Corcoran, "RITS-3 self-break water switch studies," in *Proc. 14th IEEE Int. Pulsed Power Conf.*, Dallas, TX, 2003, pp. 899–901.

[7] R. J. Adler, *Pulse Power Formulary*, North Star Research Corporation, 1989. [Online]. Available: http://www.highvoltageprobes.com/downloads

[8] I. D. Smith, "Pulse breakdown of insulator surfaces in a poor vacuum," in *1st Int. Symp. Insulation of High Voltages in Vacuum*, 1964, pp. 261–280.

[9] O. Milton, "Pulsed flashover of insulators in vacuum," *IEEE Trans. Electr. Insul.*, vol. EI-7, no. 1, pp. 9–15, 1972.

[10] D. Weidenheimer, *et al.*, "Design of a driver for the Cygnus x-ray source," in *Proc. 13th IEEE Int. Pulsed Power Conf.*, 2001, pp. 591–595.

[11] P. R. Menge, D. L. Johnson, J. E. Maenchen, D. C. Rovang, B. V. Oliver, D. V. Rose, and D. R. Welch, "Optimization of a rod pinch diode radiography source at 2.3 MV," *Rev. Sci. Instrum.*, vol. 74, no. 8, pp. 3628–3635, 2003.

[12] G. Cooperstein, *et al.*, "Theoretical modeling and experimental characterization of a rod-pinch diode," *Phys. Plasmas*, vol. 8, no. 10, pp. 4618–4636, 2001.

[13] B. V. Oliver, P. F. Ottinger, T. C. Genoni, J. W. Schumer, S. Strasburg, S. B. Swanekamp, and G. Cooperstein, "Magnetically insulated electron flow with ions with application to the rod-pinch diode," *Phys. Plasmas*, vol. 11, no. 8, pp. 3976–3991, 2004.

[14] B. V. Oliver, *et al.*, "Characterization of the rod-pinch diode x-ray source on Cygnus," in *Proc. 17th IEEE Int. Pulsed Power Conf.*, Washington, DC, 2009, pp. 11–16.

[15] D. V. Rose, *et al.*, "Numerical generation of radiographer equations for rod-pinch electron beam diodes," in *Proc. IEEE Pulsed Power Plasma Science Conf.*, Las Vegas, NV, 2001.

[16] K. D. Hahn, *et al.*, "Overview of self-magnetically pinched-diode investigations on RITS-6," *IEEE Trans. Plasma Sci.*, vol. 38, no. 10, pp. 2652–2662, 2010.